JACS
JOURNAL OF THE AMERICAN CHEMICAL SOCIETY

Article

pubs.acs.org/JACS

# Contributions of Phase, Sulfur Vacancies, and Edges to the Hydrogen Evolution Reaction Catalytic Activity of Porous Molybdenum Disulfide Nanosheets

Ying Yin,[†] Jiecai Han,[†] Yumin Zhang,[†] Xinghong Zhang,[†] Ping Xu,[*,‡] Quan Yuan,[†] Leith Samad,[§] Xianjie Wang,[⊥] Yi Wang,[∥] Zhihua Zhang,[¶] Peng Zhang,[#] Xingzhong Cao,[#] Bo Song,[*,⊥,∥] and Song Jin[*,§]

[†]Centre for Composite Materials and Structures, [‡]MIIT Key Laboratory of Critical Materials Technology for New Energy Conversion and Storage, School of Chemistry and Chemical Engineering, [⊥]Department of Physics, and [∥]Academy of Fundamental and Interdisciplinary Sciences, Harbin Institute of Technology, Harbin 150080, China

[§]Department of Chemistry, University of Wisconsin—Madison, 1101 University Avenue, Madison, Wisconsin 53706, United States

[¶]School of Materials Science and Engineering, Dalian Jiaotong University, Dalian 116028, China

[#]Institute of High Energy Physics, Chinese Academy of Sciences, Beijing 100049, China

Supporting Information

**ABSTRACT:** Molybdenum disulfide ($MoS_2$) is a promising nonprecious catalyst for the hydrogen evolution reaction (HER) that has been extensively studied due to its excellent performance, but the lack of understanding of the factors that impact its catalytic activity hinders further design and enhancement of $MoS_2$-based electrocatalysts. Here, by using novel porous (holey) metallic 1T phase $MoS_2$ nanosheets synthesized by a liquid-ammonia-assisted lithiation route, we systematically investigated the contributions of crystal structure (phase), edges, and sulfur vacancies (S-vacancies) to the catalytic activity toward HER from five representative $MoS_2$ nanosheet samples, including 2H and 1T phase, porous 2H and 1T phase, and sulfur-compensated porous 2H phase. Superior HER catalytic activity was achieved in the porous 1T phase $MoS_2$ nanosheets that have even more edges and S-vacancies than conventional 1T phase $MoS_2$. A comparative study revealed that the phase serves as the key role in determining the HER performance, as 1T phase $MoS_2$ always outperforms the corresponding 2H phase $MoS_2$ samples, and that both edges and S-vacancies also contribute significantly to the catalytic activity in porous $MoS_2$ samples. Then, using combined defect characterization techniques of electron spin resonance spectroscopy and positron annihilation lifetime spectroscopy to quantify the S-vacancies, the contributions of each factor were individually elucidated. This study presents new insights and opens up new avenues for designing electrocatalysts based on $MoS_2$ or other layered materials with enhanced HER performance.

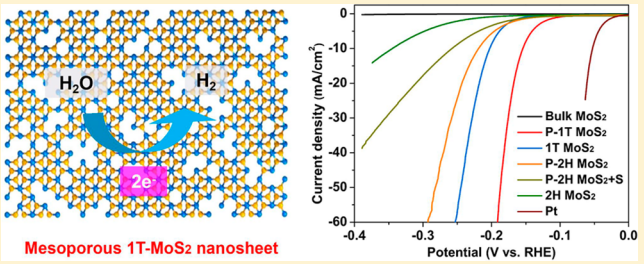


## INTRODUCTION

Hydrogen ($H_2$) is a promising clean and sustainable energy carrier and can be a suitable candidate to solve the energy and environmental crisis brought by the consumption of fossil fuels. As a result, the hydrogen evolution reaction (HER) has attracted a great deal of attention due to this urgent need for clean energy.[1−6] Noble metals, such as platinum, have excellent catalytic activity toward HER, but unfortunately, its application in large-scale hydrogen production is limited by the high cost and natural scarcity.[6] Development of new Earth-abundant electrocatalysts to replace these rare and expensive noble metal catalysts is therefore highly desirable to realize highly efficient and sustainable hydrogen production.[1] Among the Earth-abundant electrocatalysts explored,[5,6] including transition metal sulfides,[7−18] selenides,[9,19] and phosphides,[20−22] $MS_2$ (M = Mo or W) with two-dimensional (2D)-layered crystal structures are very promising catalysts with high HER catalytic activities[7,8,10−17] that potentially rival the state-of-the-art catalysts in solar-driven photoelectrochemical cells.[23]

However, debate over the key factors influencing HER catalytic activity restricts further design and improvement of the $MoS_2$-based electrocatalysts, although considerable efforts have been made during the past few years.[4,10,11,13] The HER activity of semiconducting $MoS_2$ arising from the edge sites was first confirmed;[24] therefore, many works focused on engineering higher densities of edge sites.[9,12] Conductivity and electrical contact were identified as other crucial factors,[25] and considerable effort was devoted to the improvement of either or both of these factors for enhancing HER performance of $MoS_2$ catalysts.[25−27] Recently, the nanosheets (NS) of exfoliated metallic 1T phase $MoS_2$ and $WS_2$ (with octahedral

**Received:** April 11, 2016
**Published:** June 7, 2016

  

DOI: 10.1021/jacs.6b03714
J. Am. Chem. Soc. 2016, 138, 7965−7972

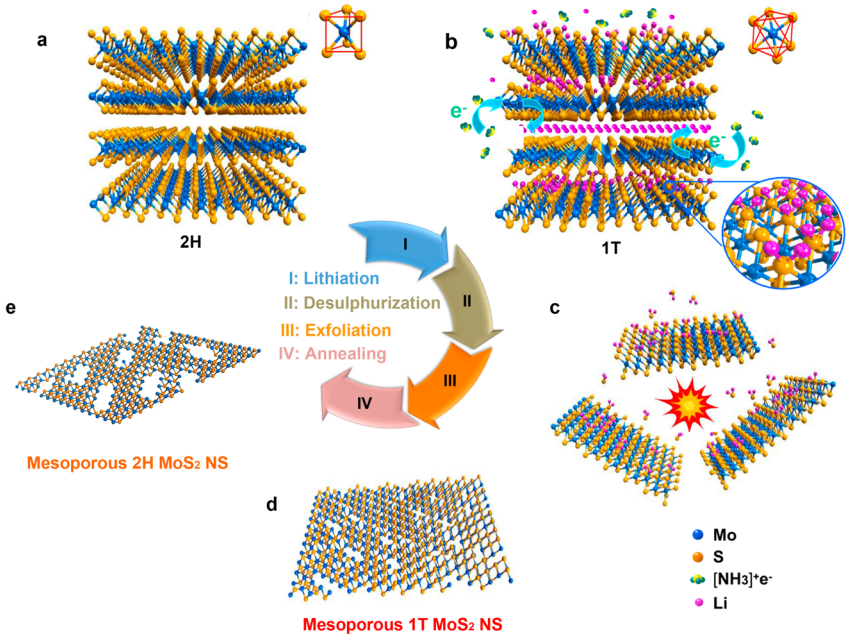


**Figure 1.** Schematic illustration of the preparation of mesoporous 1T phase $MoS_2$ nanosheets (P-1T-$MoS_2$, d) from bulk $MoS_2$ (a) by a LAAL process, including lithiation, desulfurization, and exfoliation (steps I, II, and III). Mesoporous 2H phase $MoS_2$ nanosheets (P-2H-$MoS_2$, e) can be obtained by a simple thermal annealing process from P-1T-$MoS_2$ (step IV).

structure) were demonstrated to exhibit HER catalytic performance superior to that of the semiconducting 2H phase (with trigonal-prismatic coordination) due to enhanced intrinsic catalytic activity facilitating the charge transfer kinetics.[15,17] Although subsequent theoretical[28−31] and experimental results[8,16,17,32] have confirmed the critical role of the electronic structure of the 1T-$MoS_2$ NS on the HER catalytic activity, the intrinsic mechanism for the HER enhancement in 1T-$MoS_2$ has yet to be completely elucidated, especially the roles of the edges and S-vacancies. For instance, once converted into the 1T metallic phase, are the edges of $MoS_2$ still the only catalytic active sites, as in the case of semiconducting 2H-$MoS_2$,[24] and can the defects of the 1T-$MoS_2$ be catalytically active, as well? The basal plane of the 1T phase was suggested to also be catalytically active both experimentally[32] and theoretically,[28−31] which challenges the contribution of the edges in HER activity.[29] In addition, the common defects of S-vacancies in $MoS_2$ were recently suggested to have a significant impact on HER catalytic activity.[33] It is notable that defect-rich 2H-$MoS_2$ NS with additional exposure of active edge sites exhibited enhanced HER performance,[34] and both structural and electronic benefits for enhanced HER activity in 2H phase $MoS_2$ have been realized by controllable disorder engineering and simultaneous oxygen incorporation.[14] In light of these complexities, a comprehensive and systematic investigation of these factors including phase, edges, and defects on the HER performance in both 2H and 1T phase $MoS_2$ is required.

To elucidate the contributions of edges and S-vacancies, mesoporous 1T-$MoS_2$ NS with increased content of both could meet this requirement. Recently, a liquid-ammonia-assisted lithiation (LAAL) strategy was developed to exfoliate 2D-layered materials.[35] Here, we used this strategy to synthesize novel mesoporous (holey) 1T phase $MoS_2$ NS (P-1T-$MoS_2$) with many edge sites and a large concentration of S-vacancies for the first time (Figure 1). Due to the severe desulfurization reaction between lithium and $MoS_2$, such unique mesoporous 1T phase $MoS_2$ NS not only exhibit superior catalytic performance but also serve as an ideal platform for probing the roles of phase, edges, and S-vacancies in 1T phase $MoS_2$ for HER in a holistic way. Additionally, another four representative samples including mesoporous 2H phase $MoS_2$ NS (P-2H-$MoS_2$), mesoporous 2H phase $MoS_2$ NS after sulfur compensation (P-2H-$MoS_2$+S), 1T phase $MoS_2$ NS (1T-$MoS_2$), and 2H phase $MoS_2$ NS (2H-$MoS_2$) were also prepared as model systems for a comprehensive investigation of the key factors influencing the HER catalysis of $MoS_2$. This study shows that in addition to the crystal phase that was determined to be the key factor in the HER catalytic activity of P-1T-$MoS_2$, both S-vacancies and edges also contribute significantly. The superior HER performance of the P-1T-$MoS_2$ NS can be ascribed to the cooperative effect of phase, edges, and S-vacancies. This study provides a unique opportunity to understand the intrinsic electrocatalytic nature in $MoS_2$, which allow us to achieve a superior HER performance with only pure $MoS_2$ and may pave the way for the further design of $MoS_2$-based electrocatalysts for HER and other applications.

## MATERIALS AND METHODS

**Materials.** $MoS_2$ (99.99%), metal lithium (99.999%), sulfur powder (99.99%), and *N*-methylpyrrolidone (NMP) (99.99%) were purchased from Alfa Aesar Chemical Co., Ltd. *n*-Butyl lithium (99.99%) was purchased from Aladdin. All the reagents were used without any further purification.

**Synthesis of the Materials.** *Mesoporous 1T Phase $MoS_2$ Nanosheets (P-1T-$MoS_2$).* The preparation of P-1T-$MoS_2$ from bulk $MoS_2$ materials was carried out by a three-step lithiation process using lithium−liquid ammonia medium similar to a previous work (Figure 1).[35] In step I, ∼0.5 g of bulk $MoS_2$ powder and lithium pieces with a molar ratio of 1:5 were loaded in a test tube (Figure S1a) in an argon-filled glovebox to prevent air and water contamination. The test tube was then dipped into a liquid nitrogen bath and evacuated to a pressure of $5 \times 10^{-4}$ Pa. High-purity ammonia gas was introduced into the tube and condensed into ∼12 mL of liquid, in which bulk $MoS_2$ powder was immersed (Figure S1b). The lithiation reaction started when the liquid ammonia contacted with lithium, with the blue color


DOI: 10.1021/jacs.6b03714
J. Am. Chem. Soc. 2016, 138, 7965−7972

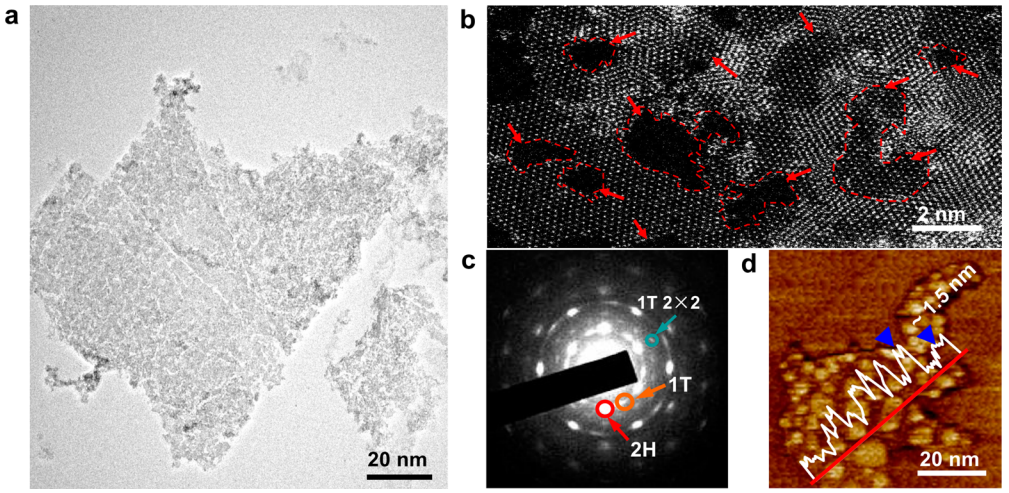


**Figure 2.** Morphology and structure characterizations of P-1T-$MoS_2$ nanosheets. (a) Low-resolution STEM image. (b) High-resolution STEM image. (c) SAED pattern corresponding to (a). (d) AFM image.

(the characteristic color of e-$(NH_3)_n$) gradually fading within 30 min (Figure S1c). In step II, the liquid ammonia was carefully removed by evaporation (Figure S1d). After the intercalation process, the Li-intercalated sample was exfoliated and ultrasonicated in deionized water for 30 min, during which a large number of bubbles were observed and an opaque suspension was produced (Figure S1e). In step III, the suspension was centrifuged at 1500 rpm to remove the residual unexfoliated $MoS_2$ particles and washed five times with deionized water to isolate the P-1T-$MoS_2$. Mesoporous 1T phase $MoS_2$ samples prepared with different molar ratios of lithium and $MoS_2$ (1:1, 2:1, 3:1, and 4:1) were also obtained following this route.

*Mesoporous 2H Phase $MoS_2$ Nanosheets (P-2H-$MoS_2$).* P-2H-$MoS_2$ was prepared through a simple annealing process from P-1T-$MoS_2$ (step IV in Figure 1). About 15 mg of as-prepared P-1T-$MoS_2$ was loaded in an alumina boat and placed in a single-zone tube furnace. The reactor was evacuated and flushed five times with high-purity argon (99.999%) before being heated to 550 °C with a ramp rate of ~5 °C/min under an argon flow of ~50 sccm and maintained at 550 °C for 2 h to ensure a complete transition from 1T to 2H phase. After that, the furnace was cooled to room temperature naturally with a flow of ~100 sccm argon.

*Sulfur-Compensated Mesoporous 2H Phase $MoS_2$ Nanosheets (P-2H-$MoS_2$+S).* An alumina boat loaded with ~8 mg of P-2H-$MoS_2$ was placed at the downstream end of the tube furnace. Then, ~1 g of sulfur powder in another alumina boat was positioned at the upstream end of the quartz tube. The distance between the two boats was ~30 cm. The tube furnace was then evacuated, and high-purity argon was flowed at ~50 sccm for 20 min while the temperature was ramped to 550 °C. The temperature was held for 2 h at 550 °C with 80 sccm argon carrier gas flow. Finally, the furnace was then naturally cooled to room temperature.

*2H Phase $MoS_2$ Nanosheets (2H-$MoS_2$).* The ultrathin 2H-$MoS_2$ was obtained by liquid exfoliation of bulk $MoS_2$ powders in NMP.[36] About 100 mg of bulk $MoS_2$ powder was dispersed in 10 mL of NMP and then ultrasonicated for 10 h followed by 24 h standing. The as-formed suspension was then centrifuged at ~3000 rpm to remove the residual unexfoliated $MoS_2$. After centrifugation, the top one-third of the suspension was extracted by pipetting.

*1T Phase $MoS_2$ Nanosheets (1T-$MoS_2$).* The preparation of 1T-$MoS_2$ was performed in an argon-filled glovebox.[15] About 0.5 g of bulk $MoS_2$ powder was soaked in 40 mL of *n*-butyl lithium (2.7 M in heptane) in a sealed vial at room temperature for >72 h and subsequently exfoliated by the reaction between the intercalated lithium with water. Excess *n*-butyl lithium was removed by rinsing the samples with dry heptane followed by deionized water.

**Structural Characterization.** X-ray diffraction (XRD) measurements were performed on a Rigaku D/max 2500 X-ray diffractometer using Cu K$\alpha$ radiation. High-angle annular dark-field imaging was performed using a JEOL ARM 200F (JEOL, Tokyo) transmission electron microscope. The attainable resolution defined by the probe-forming objective lens was <80 pm. The raw images were processed with an average background subtraction filter to reduce noise. The thickness of $MoS_2$ NS was analyzed by atomic force microscopy (AFM) on a Bruker DI MultiMode-8 system. X-ray photoelectron spectra (XPS) were recorded on an ESCALAB MKII using an Al K$\alpha$ excitation source. Raman spectra were collected on a Renishaw inVia confocal micro-Raman spectroscopy system using a TE air-cooled 576 × 400 CCD array with a 633 nm excitation laser.

**Electron Spin Resonance Spectroscopy Measurement.** Electron spin resonance (ESR) measurements were performed on a Bruker ER 200D spectrometer at room temperature. The as-prepared samples of ~28 mg were loaded in a quartz tube. The microwave frequency was maintained in the range from 9.8591 to 9.8599 GHz (X-band), and the microwave power was fixed at ~20 mW to avoid saturation.

**Positron Annihilation Measurement.** As-obtained samples were pressed into two pellets with a thickness of ~1 mm. A sandwiched structure of the sample−source−sample (e.g., P-1T-$MoS_2$/Na source/P-1T-$MoS_2$) was utilized for the positron annihilation lifetime spectroscopy (PALS) experiments performed on a fast−slow coincidence ORTEC system with a time resolution of ~195 ps at full width at half-maximum. More than two million counts were accumulated for each spectrum to reduce the statistical error in the calculation of lifetimes. Positron lifetime spectra were deconvoluted and analyzed using the LT-9 program.[37]

**Electrode Preparation and Electrochemical Characterization.** Electrochemical measurements were performed with a standard three-electrode setup (CH Instruments) using Ag/AgCl (in 3.5 M KCl solution) as the reference electrode, a graphite rod (Alfa Aesar, 99.9995%) as the counter electrode, and glassy carbon electrode (3 mm in diameter) coated with $MoS_2$ catalysts as the working electrode in a rotating disk electrode (RDE) operating at 2000 rpm. The catalyst was ultrasonically dispersed in a water−ethanol solution (v/v 3:1) containing 0.1 wt % Nafion, and a drop of the catalyst (5 $\mu$L, 2.0 mg/mL) was then transferred onto the glassy carbon electrode serving as a working electrode. The amount of deposited solid mass was calculated to be 10 $\mu$g, yielding an estimated catalyst loading of 0.14 ± 0.01 mg/cm$^2$ on the glassy carbon electrode with a geometric area of 0.07 cm$^2$. All measurements were performed in $H_2$-saturated 0.5 M $H_2SO_4$ (aq) and measured using a linear sweep with a scan rate of 5 mV s$^{-1}$. Cyclic voltammograms at various scan rates (20, 40, 60, 80, 100, 120, 140, 160, and 180 mV/s) were collected in the 0.1−0.2 V vs RHE range and used to estimate the double-layer capacitance. The electrochemical impedance spectroscopy (EIS) measurements were carried out at 250


DOI: 10.1021/jacs.6b03714
J. Am. Chem. Soc. 2016, 138, 7965−7972

mV overpotential with the frequency ranging from $10^6$ to 0.1 Hz. To better compare the true catalytic activity of the different catalysts, we used the series resistance determined from EIS experiments to correct the polarization measurements and subsequent Tafel analysis for the *iR* losses. All of the potentials were referenced to a reversible hydrogen electrode (RHE).

## RESULTS AND DISCUSSION

P-1T-$MoS_2$ was successfully synthesized by the LAAL method with a molar ratio of lithium to $MoS_2$ at 5:1, as illustrated in Figure 1 (steps I–III; see details in the Materials and Methods section), and scanning transmission electron microscopy (STEM) (Figure 2a) was used to verify the ultrathin characteristics of the as-prepared samples. Furthermore, high-resolution STEM (Figure 2b) demonstrates the porous features as denoted by the red arrows, which are in clear contrast to previously reported 1T-$MoS_2$ NS exfoliated using *n*-butyl lithium.[15] The selected area electron diffraction (SAED) pattern (Figure 2c) demonstrates a typical hexagonal spot pattern corresponding to 2H phase $MoS_2$ and an extra strong hexagonal spot at 30° between the hexagonal spots assigned to the 1T phase $MoS_2$.[38] The thickness of the as-synthesized samples was evaluated by tapping-mode AFM (Figure 2d) with a topographic height of ∼1.5 nm, suggesting the P-1T-$MoS_2$ NS have a nearly uniform thickness of ∼1–2 layers. The absence of diffraction peaks in the XRD pattern (Figure S2) clearly demonstrated that the long-range stacking order of the layers along the *c* axis was destroyed and the bulk $MoS_2$ was efficiently exfoliated into NS of single or few layers. Characterization of other porous samples prepared with different molar ratios of $MoS_2$ and lithium reveals the evolution of mesoporous structures and increased content of 1T phase $MoS_2$ with increased lithiation (Figures S3–S5 and Table S1). The P-1T-$MoS_2$ NS sample prepared with a molar ratio of lithium to $MoS_2$ at 5:1 was selected as the representative sample in the following discussion due to its saturated content of 1T phase and most prominent mesoporous features. The as-prepared P-1T-$MoS_2$ NS were subsequently converted into P-2H-$MoS_2$ NS by annealing at 550 °C in argon (step IV in Figure 1), with further annealing in sulfur vapor to (partially) compensate the S-vacancies at the same temperature and generate the P-2H-$MoS_2$+S sample. High-resolution STEM images of P-2H-$MoS_2$ and P-2H-$MoS_2$+S indicate that the porous features of P-1T-$MoS_2$ can be well maintained during the annealing process (Figure S6). For comparison, reference samples of 2H-$MoS_2$ and 1T-$MoS_2$ were obtained following previous reports.[15,36] It has been reported that the layer number of $MoS_2$ material can greatly affect its HER activity,[39−41] and here, five representative samples with the same thickness (layer number) are selected for further study in order to eliminate the influence of the layer numbers (see AFM in Figure S7).

A comparison of the Raman features of P-1T-, 1T-, P-2H-, P-2H+S-, and 2H-$MoS_2$ NS with the bulk $MoS_2$ is shown in Figure 3a. Due to the difference of the symmetry elements in crystal structures, the emergence of new Raman modes located at ∼195, 218, and 351 $cm^{-1}$ observed in 1T samples provides convincing evidence of the structural transition from pristine 2H to 1T phase $MoS_2$.[42,43] High-resolution XPS measurements then were performed to further quantify the extent of the 1T phase (Figure 3b). For 2H phase $MoS_2$, Mo 3d spectra consist of peaks around 229.4 and 232.5 eV corresponding to the Mo $3d_{5/2}$ and Mo $3d_{3/2}$ components, respectively. Notably, an

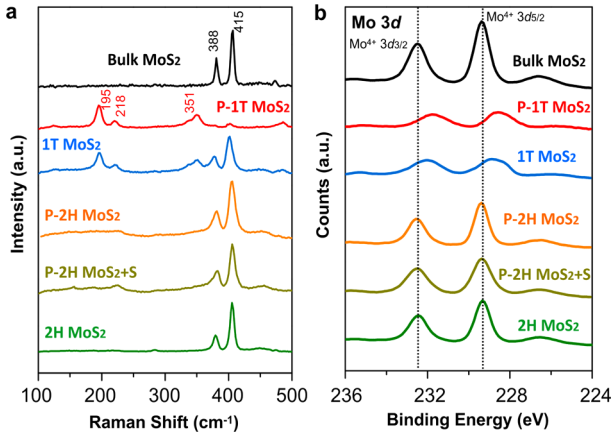


**Figure 3.** Structure characterization of the representative $MoS_2$ nanosheets. (a) Raman spectra and (b) XPS spectra for P-1T-, 1T-, P-2H-, P-2H+S-, and 2H-$MoS_2$ NS in contrast with the bulk $MoS_2$ powder.

obvious red shift for both the Mo $3d_{5/2}$ and Mo $3d_{3/2}$ peaks to the lower binding energies by ∼0.81 and 0.75 eV was observed in 1T phase $MoS_2$ and is consistent with previous reports.[32] Quantification of these peaks reveals that a maximum value of ∼82% 1T phase (Figure S8) was obtained by the LAAL route, similar to that prepared by using lithium borohydride ($LiBH_4$).[32] Similarly, with respect to the S 2p peak, an obvious shift toward lower binding energies due to a structure transition from 2H to 1T phase $MoS_2$ was also observed (Figure S9).

Next, we measured the electrochemical characteristics of various $MoS_2$ samples drop-casted on glassy carbon electrodes toward the HER catalytic performance using a RDE at a rate of 2000 rpm in 0.5 M $H_2SO_4$ in comparison to a platinum wire (see the Materials and Methods section for details). The key electrochemical results are also listed in Table 1. Figure 4a shows that P-1T-, 1T-, P-2H-, P-2H+S-, and 2H-$MoS_2$ can achieve a geometric catalytic current density of 10 $mA{\cdot}cm^{-2}$ at overpotentials ($\eta$) of 154, 202, 219, 257, and 334 mV (vs RHE after *iR* correction), respectively (see Table 1). The featureless polarization curve indicates that bulk 2H-$MoS_2$ powder provides almost negligible HER activity. From the extrapolation of the linear region of overpotential ($\eta$) versus log *j* (Figure 4b), we obtained Tafel slopes of 43, 48, 62, 82, and 106 mV per decade (after *iR* correction) for P-1T-, 1T-, P-2H-, P-2H+S-, and 2H-$MoS_2$, respectively (Table 1). Such low Tafel slope values around 40 mV/decade for P-1T- and 1T-$MoS_2$ suggest a two-electron transfer process,[44] which is smaller than that of many other reported $MoS_2$-based HER catalysts[9,12,34] and indicates efficient kinetics of $H_2$ evolution. The low overpotential of P-1T-$MoS_2$ (154 mV vs RHE for achieving 10 mA/$cm^2$) is better than or at least comparable to most of the reported phase-pure $MoS_2$-based HER catalysts (or $MoS_2$ nanocarbon composites).[14,15,32,45−47] From the intercept of the linear region of the Tafel plots, geometrical exchange current densities ($j_{0,geometrical}$) of 15.8, 12.6, 10.5, 7.9, and 3.2 $\mu A$ $cm^{-2}$ were obtained for P-1T-, 1T-, P-2H-, P-2H+S-, and 2H-$MoS_2$, respectively. The remarkable $j_{0,geometrical}$ value again suggests the excellent HER catalytic activity of P-1T-$MoS_2$, with more effective active sites originated from its unique structure characteristics.

To probe the difference in HER performance by the various $MoS_2$ samples, we measured the double-layer capacitance ($C_{dl}$) derived from the cyclic voltammogrametry measurement results


DOI: 10.1021/jacs.6b03714
J. Am. Chem. Soc. 2016, 138, 7965−7972

**Table 1. Summary of the Electrocatalytic Parameters, ESR Signal, and Positron Lifetime Parameters for Various $MoS_2$ NS Samples in Contrast with Bulk $MoS_2$ Powder**

| samples | $\eta$ (mV vs RHE) for $j = -10$ mA cm$^{-2}$ | Tafel slope (mV dec$^{-1}$) | $C_{dl}$ (mF cm$^{-2}$) | $R_{ct}$ ($\Omega$) | $j_{0,geometrical}$ ($\mu$A cm$^{-2}$) | ESR intensity of $S$ ($\times 10^3$au/mg) | positron lifetime parameters | | | |
|---|---|---|---|---|---|---|---|---|---|---|
| | | | | | | | $\tau_1$ (ps) | $I_1$ (%) | $\tau_2$ (ps) | $I_2$ (%) |
| P-1T-$MoS_2$ | 153 | 43 | 63.1 | 16 | 15.8 | 1.67 ± 0.06 | 172.4 ± 6.2 | 43.0 ± 0.4 | 346.1 ± 5.4 | 55.5 ± 0.5 |
| P-2H-$MoS_2$ | 218 | 62 | 8.2 | 280 | 10.5 | 0.81 ± 0.08 | 183.8 ± 1.1 | 43.9 ± 0.6 | 334.9 ± 2.8 | 54.5 ± 0.6 |
| P-2H-$MoS_2$+S | 257 | 82 | 5.9 | 558 | 7.9 | 1.76 ± 0.05 | 179.9 ± 6.8 | 43.2 ± 0.5 | 356.7 ± 7.2 | 52.9 ± 0.6 |
| 1T-$MoS_2$ | 203 | 48 | 23.8 | 30 | 12.6 | 3.36 ± 0.10 | 175.1 ± 4.7 | 58.9 ± 0.8 | 361.6 ± 5.4 | 40.1 ± 0.5 |
| 2H-$MoS_2$ | 343 | 106 | 0.3 | 928 | 3.2 | 1.87 ± 0.05 | 171.1 ± 1.7 | 62.2 ± 0.8 | 315.5 ± 5.5 | 36.2 ± 0.6 |
| bulk $MoS_2$ | | | | | | 1.91 ± 0.02 | 170.0 ± 4.0 | 66.4 ± 1.0 | 321.8 ± 9.5 | 32.2 ± 0.8 |

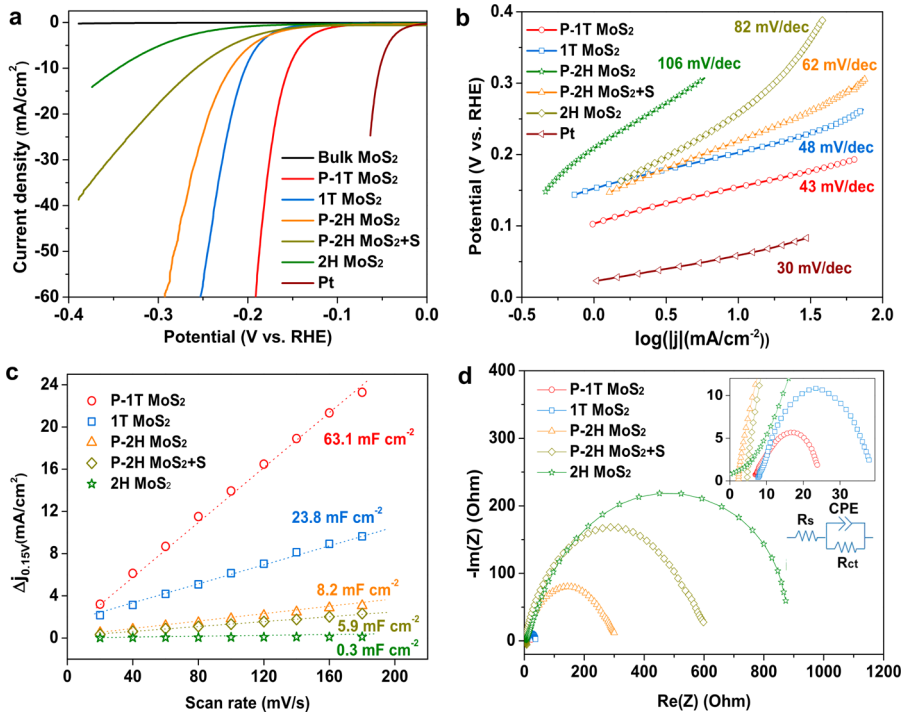


**Figure 4.** Electrochemical characterization of various $MoS_2$ samples for HER catalysis. (a) $J-V$ curves after $iR$ correction show the catalytic performance of various $MoS_2$ samples in comparison to a Pt wire. (b) Tafel plots for the data presented in (a). (c) Plots showing the extraction of the $C_{dl}$ for different $MoS_2$ samples. (d) Electrochemical impedance spectroscopy Nyquist plots for various $MoS_2$ samples. All measurement was carried out with a catalyst loading of 0.14 ± 0.01 mg/cm$^2$ on the glassy carbon electrode.

(Figure S10), which is proportional to the effective electrochemically active surface area (ECSA). Capacitive current was plotted as a function of scan rate to extract the $C_{dl}$ (Figure 4c), whose slope is equivalent to twice the value of $C_{dl}$. The calculated $C_{dl}$ values were 63.1, 23.8, 8.2, 5.9, and 0.3 mF·cm$^{-2}$ for P-1T-, 1T-, P-2H-, P-2H+S-, and 2H-$MoS_2$, respectively (Table 1). This indicates that 1T phase $MoS_2$ samples display higher exposure of catalytically active sites. Furthermore, when comparing P-1T- with 1T-$MoS_2$, introducing more edges and S-vacancies creates more HER-active sites, verifying the effect of edges and S-vacancies in HER catalysis, which was also observed for P-2H- and 2H-$MoS_2$. After sulfur compensation, the ECSA was reduced in comparison between P-2H-$MoS_2$ and P-2H-$MoS_2$+S, an indication that the S-vacancies may promote the HER activity by way of providing more active sites.

Furthermore, the electrochemical stability of the P-1T-$MoS_2$ NS was also demonstrated. Obviously, after 1000 cycles (or 20 000 s) of continuous operation, as-synthesized P-1T-$MoS_2$ NS displayed <7% (15%) decay in the electrocatalytic current density (Figure S11). We also applied EIS to provide further insight into the electrode kinetics during HER. The Nyquist plots (Figure 4d) were fitted using an equivalent circuit inset in Figure 4d to extract the charge transfer resistance ($R_{ct}$) of 16, 30, 280, 558, and 928 Ω for P-1T-, 1T-, P-2H-, P-2H+S-, and 2H-$MoS_2$, respectively (Table 1). The $R_{ct}$ of both 1T-$MoS_2$ samples is at least 1 order of magnitude smaller than that of 2H-$MoS_2$, which suggests an ultrafast Faradaic process and thus superior HER kinetics. The smallest $R_{ct}$ from P-1T-$MoS_2$ is attributed to its unique structure in addition to phase, where more edges and S-vacancies are introduced during the LAAL lithiation process. Furthermore, sulfur compensation almost doubles the $R_{ct}$ value of P-2H-$MoS_2$+S as compared to that of P-2H-$MoS_2$, which is another indication that S-vacancies also facilitate charge transfer during HER. The catalytic turnover frequency has also been estimated (see Supporting Information),[48] which is about 0.5 $H_2$ s$^{-1}$ per surface site for the representative P-1T-$MoS_2$ sample at an overpotential of 153 mV (a current density of 10 mA cm$^{-2}$).

The comprehensive comparison of the electrochemical performances from these representative $MoS_2$ samples above (Table 1) reveals several important points. First, the 1T phase (including both conventional 1T and porous 1T) $MoS_2$ always


DOI: 10.1021/jacs.6b03714
J. Am. Chem. Soc. 2016, 138, 7965−7972

demonstrates HER catalytic activity superior to that of the corresponding 2H phase, consistent with previous studies.[15,16,32] Of note is that increasing the density of edges, as found in the P-1T-$MoS_2$ and P-2H-$MoS_2$ samples, can further improve the catalytic performance because the edge-terminated features can ensure an isotropic electron transport as compared to their bulk morphologies.[45] More importantly, porous 1T-$MoS_2$ does perform better than 1T-$MoS_2$, which suggests that the edges in 1T-$MoS_2$ NS are still important for catalytic activity. However, the contribution of S-vacancies to the HER catalysis also should not be neglected as it manifests as a decrease in the overpotential of P-2H-$MoS_2$+S when sulfur was replenished to P-2H-$MoS_2$ to reduce S-vacancies. Though quantitative determination of the edges is not available currently, the positive effect of S-vacancies has been clearly revealed in our case. These electrochemical data clearly indicate that the HER activity of the $MoS_2$ samples is dominated by a cooperative effect of crystal phase, concentration of edges, and S-vacancies.

To further study the contribution of S-vacancies in $MoS_2$ for HER, we employed ESR spectroscopy to provide fingerprint information for a paramagnetic signal. Among them, the *S* signal observed at ~3500 G ($g$ = 1.91−2.003) can be ascribed to the contribution from Mo−S dangling bonds,[49,50] where a higher intensity indicates less S-vacancies. As shown in Figure 5

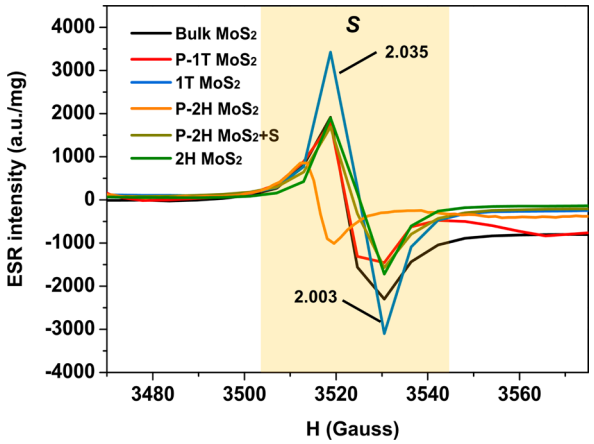


**Figure 5.** Electron spin resonance spectra for various $MoS_2$ samples. The *S* signal is ascribed to the contribution from Mo−S dangling bonding, and a higher intensity indicates lower concentration of S-vacancies.

and Table 1, the *S* signal increases significantly from pristine bulk $MoS_2$ (~$1.91 \times 10^3$ au/mg) to 1T-$MoS_2$ (~$3.36 \times 10^3$ au/mg) due to the expansion of the Mo−S bond during the formation of the 1T phase. Significant reduction in *S* signal intensity of P-1T-$MoS_2$ as compared to that of 1T-$MoS_2$ reveals an obvious increase of S-vacancies introduced during the harsh lithiation process of LAAL. The annealing process that transformed the crystal structure from P-1T- to P-2H-$MoS_2$, accompanied by partial reconstruction of Mo−S bonding, led to a significantly decreased *S* signal from ~$1.67 \times 10^3$ to ~$0.81 \times 10^3$ au/mg. Subsequently, it follows that the *S* signal was enhanced from P-2H-$MoS_2$ to P-2H-$MoS_2$+S as the concentration of S-vacancies was reduced after sulfur compensation. Furthermore, with the increase in the molar ratio of $MoS_2$ to lithium from 1:1 to 1:5 in the various porous samples prepared via LAAL, the value of the *S* signal exhibited a decrease from ~$3.22 \times 10^3$ to ~$1.67 \times 10^3$ au/mg (Figure S12 and Table S2), suggesting a gradual increase of the S-vacancy concentration in P-1T-$MoS_2$ samples.

To provide direct information on the S-vacancies with parts per million level sensitivity in various $MoS_2$ samples, we further employed PALS.[51,52] Normally, the positron lifetime spectra (Figure S13) can be fit to an exponential function of three components corresponding to different annihilation sites. Herein, the long lifetime of more than 2 ns, usually assigned to the annihilations at voids/surface, was not considered due to its negligible contribution.[53] Then, we only consider two lifetime components in PALS spectra, $\tau_1$ and $\tau_2$, with relative intensities, $I_1$ and $I_2$ (Table 1). The predominant shorter component ($\tau_1$, 170 ± 5 ps) was assigned to the bulk lifetime of $MoS_2$, while another longer life component ($\tau_2$, 321.8 ± 7 ps) was attributed to the positron annihilation corresponding to S-vacancies.[54,55] This is what we will focus our discussion on. The relative concentration of S-vacancies can be determined from the relative intensity *I*. $I_2$ of 2H-$MoS_2$ is slightly higher than that of bulk $MoS_2$, revealing very limited S-vacancies in 2H-$MoS_2$. After lithiation, the S-vacancies become dominant in the P-1T, P-2H, and P-2H+S samples, with $I_2$ exceeding ~52%. Furthermore, as shown in Table S2, the content of S-vacancies gradually increases with increasing ratio of lithium to $MoS_2$ in various porous $MoS_2$ samples prepared via the LAAL process due to the enhanced desulfurization reaction, in good agreement with the ESR results above. From P-1T to P-2H, it was found that although the quantity of Mo−S bonding decreased, the content of S-vacancies remained unchanged. This further confirms the critical role of phase for HER catalytic activity of $MoS_2$, while the contributions from edges and S-vacancies are kept constant. When comparing P-2H and P-2H +S, the slight decrease in $I_2$ indicates that S-vacancies were partially restored by sulfur compensation successfully. It is worth noting that not all of the sulfur was utilized to fill in the S-vacancies but to form new Mo−S dangling bonds simultaneously, as revealed by an increased *S* signal in ESR from ~$0.81 \times 10^3$ to $1.76 \times 10^3$ au/mg. Finally, from P-2H+S- to P-2H-$MoS_2$, it can observed that with all other factors being equal, the increased S-vacancy concentration can lead to enhanced HER catalytic activity, independent of whether the S-vacancies come from the edges or the basal plane, which is consistent with a recent report.[33]

Both ESR and PALS characterization techniques above provide convincing evidence to reveal and quantify S-vacancies and confirm their influence on HER catalysis. As a result, we can conclude that (i) comparing P-1T- with P-2H-$MoS_2$, similar $I_2$ values suggest that phase rather than edges or S-vacancies dominates the electrocatalytic activity of $MoS_2$; (ii) comparing P-1T- with 1T-$MoS_2$, both edges and S-vacancies also play important roles in determining the superior HER performance in P-1T-$MoS_2$; (iii) from comparing P-2H and P-2H+S with identical content of edges and the same crystal phase, increased content of S-vacancies improves the HER performance. The enhanced catalytic activity and superior HER catalytic performance in P-1T-$MoS_2$ were therefore attributed to the cooperative effect of phase, edges, and S-vacancies.

## ■ CONCLUSIONS

In summary, we have used a series of representative (and in some cases unique) samples, including porous 1T-, porous 2H-, porous 2H+S-, 1T-, and 2H-$MoS_2$ nanosheets, to systematically probe the contributions of phase, edges, and S-vacancies to the


DOI: 10.1021/jacs.6b03714
J. Am. Chem. Soc. 2016, 138, 7965−7972

HER catalytic activity by utilizing Raman, XPS, and electrochemical impedance spectroscopy, as well as electron spin resonance and positron annihilation lifetime spectroscopy. These comprehensive studies conclusively show that the crystal phase serves as the key role in determining the HER catalytic activity in both conventional 1T and porous 1T phase $MoS_2$ nanosheets and also that the edges and S-vacancies make significant contributions to the electrocatalytic properties of $MoS_2$. Due to the cooperative effects of the phase, S-vacancies, and edges, high intrinsic HER activity can be obtained on the porous 1T-$MoS_2$ nanosheets, with $\eta$ = 153 mV vs RHE for $j$ = −10 mA·cm$^{-2}$, a Tafel slope of 43 mV per decade, and higher electrochemically active surface area. This study provides new and comprehensive insights to reveal the critical factors that influence the catalytic activity of $MoS_2$, which will enable the design and improvement of Earth-abundant electrocatalysts based on $MoS_2$ and other layered materials with further enhanced catalytic performance.

## ■ ASSOCIATED CONTENT

### Supporting Information

The Supporting Information is available free of charge on the ACS Publications website at DOI: 10.1021/jacs.6b03714.

Figures S1−S13, Tables S1 and S2, and estimation of catalytic turnover frequency (PDF)

## ■ AUTHOR INFORMATION


### Corresponding Authors

*pxu@hit.edu.cn
*songbo@hit.edu.cn
*jin@chem.wisc.edu


### Notes

The authors declare no competing financial interest.

## ■ ACKNOWLEDGMENTS

This work is supported by the Major State Basic Search Program (No. 2014CB46505), Science Fund for Creative Research Groups of the National Natural Science Foundation of China (Grant No. 10821201), and the National Natural Science Foundation of China (Grant Nos. 51172055, 51372056, 51472064, and 21471039), Fundamental Research Funds for the Central University (Grant Nos. HIT.BRETIII.201220, HIT.NSRIF.2012045, HIT.ICRST.2010008, PIRS of HITA201502), International Science & Technology Cooperation Program of China (2012DFR50020) and the Program for New Century Excellent Talents in University (NCET-13-0174). S.J. thanks support by the U.S. Department of Energy, Office of Basic Energy Sciences, Division of Materials Sciences and Engineering, under Award DE-FG02-09ER46664.

## ■ REFERENCES


(1) Turner, J. A. *Science* **2004**, *305*, 972.
(2) Lewis, N. S.; Nocera, D. G. *Proc. Natl. Acad. Sci. U. S. A.* **2006**, *103*, 15729.
(3) Hou, Y.; Abrams, B. L.; Vesborg, P. C. K.; Björketun, M. E.; Herbst, K.; Bech, L.; Setti, A. M.; Damsgaard, C. D.; Pedersen, T.; Hansen, O.; Rossmeisl, J.; Dahl, S.; Nørskov, J. K.; Chorkendorff, I. *Nat. Mater.* **2011**, *10*, 434.
(4) Laursen, A. B.; Kegnaes, S.; Dahl, S.; Chorkendorff, I. *Energy Environ. Sci.* **2012**, *5*, 5577.
(5) Morales-Guio, C. G.; Stern, L.-A.; Hu, X. *Chem. Soc. Rev.* **2014**, *43*, 6555.
(6) Faber, M. S.; Jin, S. *Energy Environ. Sci.* **2014**, *7*, 3519.
(7) Hinnemann, B.; Moses, P. G.; Bonde, J.; Jørgensen, K. P.; Nielsen, J. H.; Horch, S.; Chorkendorff, I.; Nørskov, J. K. *J. Am. Chem. Soc.* **2005**, *127*, 5308.
(8) Lukowski, M. A.; Daniel, A. S.; English, C. R.; Meng, F.; Forticaux, A.; Hamers, R. J.; Jin, S. *Energy Environ. Sci.* **2014**, *7*, 2608.
(9) Kong, D.; Wang, H.; Cha, J. J.; Pasta, M.; Koski, K. J.; Yao, J.; Cui, Y. *Nano Lett.* **2013**, *13*, 1341.
(10) Morales-Guio, C. G.; Hu, X. *Acc. Chem. Res.* **2014**, *47*, 2671.
(11) Benck, J. D.; Hellstern, T. R.; Kibsgaard, J.; Chakthranont, P.; Jaramillo, T. F. *ACS Catal.* **2014**, *4*, 3957.
(12) Kibsgaard, J.; Chen, Z.; Reinecke, B. N.; Jaramillo, T. F. *Nat. Mater.* **2012**, *11*, 963.
(13) Vrubel, H.; Hu, X. *ACS Catal.* **2013**, *3*, 2002.
(14) Xie, J.; Zhang, J.; Li, S.; Grote, F.; Zhang, X.; Zhang, H.; Wang, R.; Lei, Y.; Pan, B.; Xie, Y. *J. Am. Chem. Soc.* **2013**, *135*, 17881.
(15) Lukowski, M. A.; Daniel, A. S.; Meng, F.; Forticaux, A.; Li, L.; Jin, S. *J. Am. Chem. Soc.* **2013**, *135*, 10274.
(16) Wang, H.; Lu, Z.; Xu, S.; Kong, D.; Cha, J. J.; Zheng, G.; Hsu, P.-C.; Yan, K.; Bradshaw, D.; Prinz, F. B.; Cui, Y. *Proc. Natl. Acad. Sci. U. S. A.* **2013**, *110*, 19701.
(17) Voiry, D.; Yamaguchi, H.; Li, J.; Silva, R.; Alves, D. C. B.; Fujita, T.; Chen, M.; Asefa, T.; Shenoy, V. B.; Eda, G.; Chhowalla, M. *Nat. Mater.* **2013**, *12*, 850.
(18) Faber, M. S.; Dziedzic, R.; Lukowski, M. A.; Kaiser, N. S.; Ding, Q.; Jin, S. *J. Am. Chem. Soc.* **2014**, *136*, 10053.
(19) Kong, D.; Cha, J. J.; Wang, H.; Lee, H. R.; Cui, Y. *Energy Environ. Sci.* **2013**, *6*, 3553.
(20) Popczun, E. J.; Read, C. G.; Roske, C. W.; Lewis, N. S.; Schaak, R. E. *Angew. Chem., Int. Ed.* **2014**, *53*, 5427.
(21) Popczun, E. J.; McKone, J. R.; Read, C. G.; Biacchi, A. J.; Wiltrout, A. M.; Lewis, N. S.; Schaak, R. E. *J. Am. Chem. Soc.* **2013**, *135*, 9267.
(22) Caban-Acevedo, M.; Stone, M. L.; Schmidt, J. R.; Thomas, J. G.; Ding, Q.; Chang, H.-C.; Tsai, M.-L.; He, J.-H.; Jin, S. *Nat. Mater.* **2015**, *14*, 1245.
(23) McKone, J. R.; Lewis, N. S.; Gray, H. B. *Chem. Mater.* **2014**, *26*, 407.
(24) Jaramillo, T. F.; Jørgensen, K. P.; Bonde, J.; Nielsen, J. H.; Horch, S.; Chorkendorff, I. *Science* **2007**, *317*, 100.
(25) Li, Y.; Wang, H.; Xie, L.; Liang, Y.; Hong, G.; Dai, H. *J. Am. Chem. Soc.* **2011**, *133*, 7296.
(26) Tan, Y.; Liu, P.; Chen, L.; Cong, W.; Ito, Y.; Han, J.; Guo, X.; Tang, Z.; Fujita, T.; Hirata, A.; Chen, M. W. *Adv. Mater.* **2014**, *26*, 8023.
(27) Islam, M. R.; Kang, N.; Bhanu, U.; Paudel, H. P.; Erementchouk, M.; Tetard, L.; Leuenberger, M. N.; Khondaker, S. I. *Nanoscale* **2014**, *6*, 10033.
(28) Putungan, D. B.; Lin, S.-H.; Kuo, J.-L. *Phys. Chem. Chem. Phys.* **2015**, *17*, 21702.
(29) Tsai, C.; Chan, K.; Nørskov, J. K.; Abild-Pedersen, F. *Surf. Sci.* **2015**, *640*, 133.
(30) Fan, X.-L.; Yang, Y.; Xiao, P.; Lau, W.-M. *J. Mater. Chem. A* **2014**, *2*, 20545.
(31) Lin, S.-H.; Kuo, J.-L. *Phys. Chem. Chem. Phys.* **2015**, *17*, 29305.
(32) Voiry, D.; Salehi, M.; Silva, R.; Fujita, T.; Chen, M.; Asefa, T.; Shenoy, V. B.; Eda, G.; Chhowalla, M. *Nano Lett.* **2013**, *13*, 6222.
(33) Li, H.; Tsai, C.; Koh, A. L.; Cai, L.; Contryman, A. W.; Fragapane, A. H.; Zhao, J.; Han, H. S.; Manoharan, H. C.; Abild-Pedersen, F.; Norskov, J. K.; Zheng, X. *Nat. Mater.* **2016**, *15*, 48.
(34) Xie, J.; Zhang, H.; Li, S.; Wang, R.; Sun, X.; Zhou, M.; Zhou, J.; Lou, X. W.; Xie, Y. *Adv. Mater.* **2013**, *25*, 5807.
(35) Yin, Y.; Han, J.; Zhang, X.; Zhang, Y.; Zhou, J.; Muir, D.; Sutarto, R.; Zhang, Z.; Liu, S.; Song, B. *RSC Adv.* **2014**, *4*, 32690.
(36) Coleman, J. N.; Lotya, M.; O'Neill, A.; Bergin, S. D.; King, P. J.; Khan, U.; Young, K.; Gaucher, A.; De, S.; Smith, R. J.; Shvets, I. V.; Arora, S. K.; Stanton, G.; Kim, H.-Y.; Lee, K.; Kim, G. T.; Duesberg, G. S.; Hallam, T.; Boland, J. J.; Wang, J. J.; Donegan, J. F.; Grunlan, J. C.; Moriarty, G.; Shmeliov, A.; Nicholls, R. J.; Perkins, J. M.; Grieveson, E.




DOI: 10.1021/jacs.6b03714
J. Am. Chem. Soc. 2016, 138, 7965−7972

M.; Theuwissen, K.; McComb, D. W.; Nellist, P. D.; Nicolosi, V. *Science* **2011**, *331*, 568.
(37) Kansy, J.; Hanc, A.; Pająk, L.; Giebel, D. *Phys. Status Solidi C* **2009**, *6*, 2326.
(38) Wypych, F.; Schollhorn, R. *J. Chem. Soc., Chem. Commun.* **1992**, 1386.
(39) Yu, Y.; Huang, S.-Y.; Li, Y.; Steinmann, S. N.; Yang, W.; Cao, L. *Nano Lett.* **2014**, *14*, 553.
(40) Laursen, A. B.; Vesborg, P. C. K.; Chorkendorff, I. *Chem. Commun.* **2013**, *49*, 4965.
(41) Seo, B.; Jung, G. Y.; Sa, Y. J.; Jeong, H. Y.; Cheon, J. Y.; Lee, J. H.; Kim, H. Y.; Kim, J. C.; Shin, H. S.; Kwak, S. K.; Joo, S. H. *ACS Nano* **2015**, *9*, 3728.
(42) Yang, D.; Sandoval, S. J.; Divigalpitiya, W. M. R.; Irwin, J. C.; Frindt, R. F. *Phys. Rev. B: Condens. Matter Mater. Phys.* **1991**, *43*, 12053.
(43) Jiménez Sandoval, S.; Yang, D.; Frindt, R. F.; Irwin, J. C. *Phys. Rev. B: Condens. Matter Mater. Phys.* **1991**, *44*, 3955.
(44) Conway, B. E.; Tilak, B. V. *Electrochim. Acta* **2002**, *47*, 3571.
(45) Gao, M.-R.; Chan, M. K. Y.; Sun, Y. *Nat. Commun.* **2015**, *6*, 7493.
(46) Smith, A. J.; Chang, Y.-H.; Raidongia, K.; Chen, T.-Y.; Li, L.-J.; Huang, J. *Adv. Energy Mater.* **2014**, *4*, 1400398.
(47) Li, Y.; Wang, H.; Xie, L.; Liang, Y.; Hong, G.; Dai, H. *J. Am. Chem. Soc.* **2011**, *133*, 7296.
(48) Zhuo, J.; Caban-Acevedo, M.; Liang, H.; Samad, L.; Ding, Q.; Fu, Y.; Li, M.; Jin, S. *ACS Catal.* **2015**, *5*, 6355.
(49) Deroide, B.; Belougne, P.; Zanchetta, J. V. *J. Phys. Chem. Solids* **1987**, *48*, 1197.
(50) Deroide, B.; Bensimon, Y.; Belougne, P.; Zanchetta, J. V. *J. Phys. Chem. Solids* **1991**, *52*, 853.
(51) Alatalo, M.; Barbiellini, B.; Hakala, M.; Kauppinen, H.; Korhonen, T.; Puska, M. J.; Saarinen, K.; Hautojärvi, P.; Nieminen, R. M. *Phys. Rev. B: Condens. Matter Mater. Phys.* **1996**, *54*, 2397.
(52) Tuomisto, F.; Makkonen, I. *Rev. Mod. Phys.* **2013**, *85*, 1583.
(53) Liang, L.; Li, K.; Xiao, C.; Fan, S.; Liu, J.; Zhang, W.; Xu, W.; Tong, W.; Liao, J.; Zhou, Y.; Ye, B.; Xie, Y. *J. Am. Chem. Soc.* **2015**, *137*, 3102.
(54) Ohdaira, T.; Suzuki, R.; Mikado, T.; Ohgaki, H.; Chiwaki, M.; Yamazaki, T.; Hasegawa, M. *Appl. Surf. Sci.* **1996**, *100−101*, 73.
(55) Viswanath, R. N.; Ramasamy, S. *J. Mater. Sci.* **1990**, *25*, 5029.


DOI: 10.1021/jacs.6b03714
*J. Am. Chem. Soc.* 2016, 138, 7965−7972